606 J. Opt. Soc. Am. B/Vol. 2, No. 4/April 1985

Coherent time-domain far-infrared spectroscopy

D. H. Auston and K. P. Cheung

AT&T Bell Laboratories, Murray Hill, New Jersey 07974

Received December 11, 1984; accepted December 14, 1984

A new approach to far-infrared spectroscopy is described that uses extremely short far-infrared pulses to measure the dielectric properties of materials. Optical rectification of femtosecond optical pulses is used to produce a Čerenkov cone of pulsed far-infrared radiation of approximately one cycle in duration in the terahertz spectral range. The coherent detection of the electric field of these far-infrared pulses by electro-optic sampling provides a capability for measuring precise changes in the shape of the waveform following reflection or transmission from materials. This method, which is equivalent to having a tunable laser in the spectral range from 0.1 to 2 THz, is illustrated by the measurement of the dielectric response of a solid-state plasma in n-type germanium and a GaAs/GaAlAs multiquantum-well superlattice.

INTRODUCTION

The far-infrared region of the electromagnetic spectrum is of crucial importance to the study of elementary excitations in solids.[1] Superconducting band gaps, lattice resonances, and impurity levels are examples of material properties whose excitation energies lie in the spectral range from a fraction of 1 TH to a few terahertz (1 THz $\equiv 10^{12}$ sec$^{-1} \equiv 4.14$ mV $\equiv 300$ μm $\equiv 33$ cm$^{-1} \equiv 48$ K). Although the introduction of Fourier-transform spectrometers has greatly aided the exploration of the far infrared, it is clear that tunable coherent sources of radiation with greater brightness are needed. This is particularly true for the study of nonlinear and transient phenomena. For this reason, extensive work has been done on the development of free-electron lasers operating in the far infrared, and it is expected that these instruments will soon be available to the spectroscopist. The detection of far-infrared radiation also allows considerable room for improvement with regard to both sensitivity and speed of response.

In this paper we describe a new approach to far-infrared spectroscopy that uses nonlinear optics and femtosecond optical pulses to generate and measure extremely short electromagnetic transients whose frequency spectra span a large portion of the entire far-infrared spectral range. A novel feature of this method is the use of these coherent continuum far-infrared pulses to make measurements in the time domain that are entirely equivalent to having a tunable monochromatic source covering the same spectral range. The first part of the paper summarizes the generation and detection of far-infrared pulses in electro-optic materials. The use of these pulses for coherent time-domain far-infrared spectroscopy is then described in detail, followed by two illustrations of its application to the measurement of the dielectric response of semiconductors. The paper concludes with a discussion of the unique advantages of this approach, its limitations, and further improvements and applications.

FAR-INFRARED GENERATION BY THE ELECTRO-OPTIC ČERENKOV EFFECT

It was recently proposed[2,3] and demonstrated[4] that, under suitable conditions, the propagation of femtosecond optical pulses in electro-optic materials should be accompanied by the radiation of an extremely fast electromagnetic transient. This phenomenon, which arises from the inverse electro-optic effect,[5] produces a Čerenkov cone of pulsed radiation having a duration of approximately one cycle and a frequency in the terahertz range. Although this effect closely resembles the classical Čerenkov radiation from relativistic charged particles in dielectric media, its physical basis has some unique distinguishing features. Most important, it is a nonlinear optical effect, arising from a second-order nonlinear polarization, and consequently requires a lack of inversion symmetry in the host material. Also, the charge state of the effective source is neutral, being a dipole moment rather than a point charge. The velocity of the source, however, does exceed the radiation velocity because of the additional contribution to the low-frequency dielectric response from the infrared lattice vibrations. As is indicated in Fig. 1, this is expected to produce a characteristic cone of radiation in the form of a shock wave. Unlike with classical Čerenkov radiation, however, the radiation source is spatially extended, being proportional to the intensity envelope of the optical pulse. Consequently the details of the radiation field are expected to depend sensitively on both the duration and the beam waist of the optical pulse. A discussion of these effects, based on an analysis of this phenomenon, is given in Refs. 2 and 3. We summarize here only the salient features of this work.

An analysis of the electro-optic Čerenkov radiation process[2,3] predicts the following expression for the time variation of the electric field:

$$E(t) = \frac{n_0^2 r_{33} W_p}{c^2 \tau^2} \left(\frac{\sqrt{2} \cot \theta_c}{v \tau r_\perp} \right)^{1/2} \times U\left(-2, -\frac{\sqrt{2}t}{\tau}\right) \exp\left(-\frac{t^2}{2\tau^2}\right), \quad (1)$$

where W_p is the optical pulse energy, n_0 and v are the optical index of refraction and the group velocity, $r_\perp$ is the radial distance from the beam axis, θ_c is the Čerenkov cone angle $[=\cos^{-1}(c/v\sqrt{\epsilon_3})]$, r_{33} is the electro-optic coefficient, $U(-2, x)$ is the parabolic cylinder function of order -2, and the parameter τ is defined by the relationship

0740-3224/85/040606-07$02.00

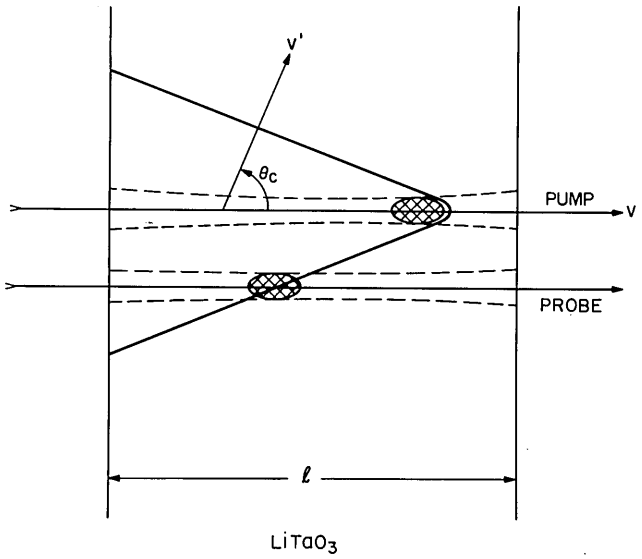

Fig. 1. Schematic of the experiment used to generate and detect short far-infrared bursts by Čerenkov radiation from femtosecond optical pulses in lithium tantalate. The Čerenkov cone of radiation propagates away from the pump pulse in a direction θ_c with a velocity that is determined by the ratio of the low-frequency index of refraction to the optical group velocity. A probe pulse measures the small birefringence that is due to the electro-optic effect induced by the electric field of the far-infrared transient as it moves in synchronism with the Čerenkov wave front.

$$\tau = \left(\tau_p{}^2 + \frac{w^2 \tan^2 \theta_c}{v^2}\right)^{1/2}, \tag{2}$$

where τ_p is the $1/e$ half-width of the duration of the optical pulse and w is the $1/e$ beam radius (both assumed to have Gaussian profiles). The theory neglects dispersion and assumes that the point of observation is much greater than the optical beam waist. A unique feature of this result is the variation of the electric-field amplitude with the inverse 5/2 power of the pulse-width parameter τ (the field intensity varies as the inverse fifth power of τ). This makes the efficiency of this process as well as its speed much more attractive when extremely short optical pulses are used. A second aspect of the theory is the contribution to the infrared pulse duration from the beam waist of the optical pulse, as illustrated by expression (2). This means that tight focusing is necessary to produce extremely fast pulses.

The frequency spectrum of the pulse is given by the expression

$$E(\omega) = \omega^{3/2} \exp\left(-\frac{\omega^2 \tau^2}{4}\right). \tag{3}$$

Since the pulse is of the order of one cycle in duration, the spectrum is extremely broad. It peaks at a frequency equal to

$$f_m = \sqrt{3}/(2\pi\tau). \tag{4}$$

Although many electro-optic materials can be used for this purpose, lithium tantalate has some particularly desirable features. First, it has a relatively large electro-optic coefficient along its polar axis equal to 2.8×10^{-11} m/V.[6] Second, it has a very low anisotropy of both its optical and low-frequency dielectric constants (0.2 and 0.5%, respectively). Third, it has a relatively large region of transparency in the far infrared, extending from dc to the transverse optic lattice resonance at 6 THz.[7]

Femtosecond optical pulses were obtained from a colliding-pulse mode-locked ring dye laser.[8] Their duration, measured by second-harmonic autocorrelation, was 100 fsec (full width at half-maximum), and their center wavelength was 625 nm. A relatively low pulse energy of only 10^{-10} J at a repetition rate of 150 MHz was sufficient for the experiments described in this paper.

COHERENT FAR-INFRARED DETECTION

The detection of the infrared pulses is accomplished with the use of a second femtosecond optical pulse, which is synchronized and delayed with respect to the generating pulse, as illustrated in Fig. 1. This configuration exploits a novel symmetry arising from the use of the electro-optic effect for both generation and detection. In the case of the generating pulse it is the inverse electro-optic effect that produces the nonlinear polarization responsible for the radiation field, and in the detection process it is the direct electro-optic effect that is used to measure the small birefringence produced by the electric field of the radiation pulse. This latter technique, known as electro-optic sampling,[9] was previously used to measure subpicosecond electrical transients in traveling-wave electro-optic transmission lines.

An example of the waveform measured by this technique is shown in Fig. 2. It is extremely fast and represents a single cycle of a frequency of approximately 1 THz. Its shape closely resembles the theoretical waveform predicted by expression (1). By calibrating the detection method, the electric-field amplitude was estimated to be 10 V/cm. For this measurement both optical pulses were focused on a sample of lithium tantalate through a common lens and were carefully aligned to propagate parallel through the crystal. The generating pulse was polarized parallel to the c axis of the crystal (out of

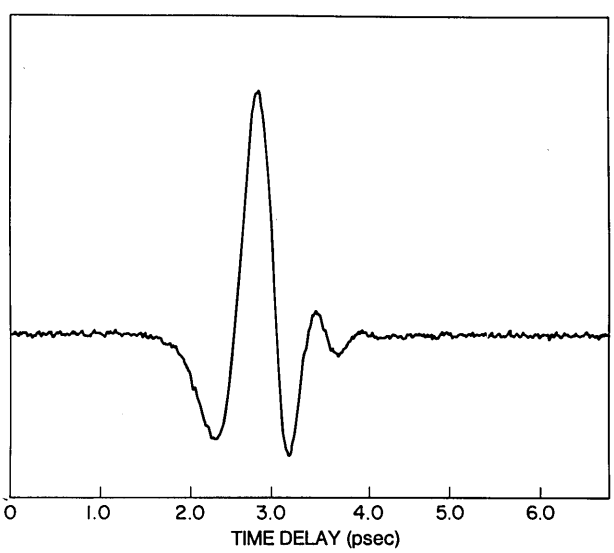

Fig. 2. Experimental observation of the electric-field waveform of the far-infrared transient measured by the method illustrated in Fig. 1. A lithium tantalate crystal 1 mm in length was used with 100-fsec optical pulses focused to a beam waist of approximately 7 μm. The peak amplitude of the electric field was approximately 10 V/cm. The true shape of the far-infrared pulse is faster than the result shown here because of the convolution with the probe pulse.

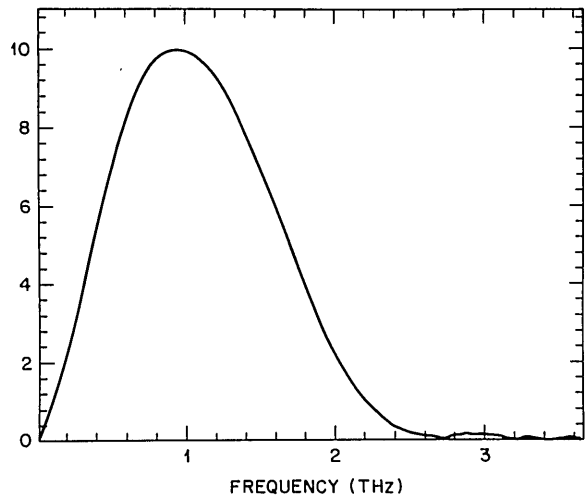

Fig. 3. Fourier spectrum of the experimental waveform in Fig. 2.

the plane of Fig. 1) to produce a radiation field polarized in the same direction by the r_{33} electro-optic coefficient. The probing pulse was polarized 45 deg to the c axis of the lithium tantalate, and the static birefringence was compensated by a Soleil–Babinet compensator placed after the crystal. A calcite Glan–Thompson polarizing prism was used as an analyzer to separate the two orthogonally polarized components of the transmitted pulse. Differential detection of these two signals was used to measure the rotation of the axis of polarization of the transmitted optical pulse arising from the birefringence produced by the radiation field. The compensator was used to bias the detection system at the point of maximum incremental sensitivity where the response is linearly proportional to the electric field of the radiated wave.

A unique feature of the use of optical pulses for both generating and detecting the radiation field is the automatic synchronism of the velocities of the radiation field and the probing pulse. As is indicated in Fig. 1, the probing pulse surfs along the Čerenkov wave front, enabling it to measure the electric field at a stationary point in the waveform by integrating the birefringence along the entire path through the crystal. To plot out the shape of the waveform, the timing of the probing pulse was delayed or advanced relative to the generating pulse by introducing a variable path length between them.

The measurement technique introduces an additional broadening to the observed waveform that is due to the spatial and temporal convolution between the electric field and the probing pulse. If the generating and probing pulses are identical, and no other sources of broadening are present, this would introduce an additional factor of $\sqrt{2}$ into the parameter τ in expression (2).

A crucial aspect of the detection method is that it is coherent, i.e., it measures the electric-field amplitude, not the intensity profile of the pulse. Also, the lack of time jitter between the generation and detection processes means that small time displacements have physical significance. This means that the waveform is well defined with respect to both its amplitude and its phase. Consequently, we can Fourier transform time-domain waveforms to obtain their complex frequency spectra. The frequency spectrum of the waveform in Fig. 2, determined by a numerical Fourier transform, is shown in Fig. 3. The spectral content of the pulse is extremely broad, extending from dc to 2.5 THz.

COHERENT TIME-DOMAIN SPECTROSCOPY

The concept of coherent time-domain spectroscopy is not new. It is implicit in electronic measurements that use impulse excitation to determine the dispersive properties of a circuit or device. In this case, the response manifests itself as a distortion or broadening of the pulse as measured in real time on a oscilloscope. Since the oscilloscope is a coherent detector, the frequency response can be determined by a simple numerical Fourier transform. This approach, however, is usually not possible in optics since most optical detectors are not coherent: They measure only the intensity envelope of the signal and do not trace out the true electric-field amplitude. The essential information about the phase of the carrier is usually lost. If, however, as in our case, a coherent detection scheme can be employed, the full equivalency of time and frequency applies. This means that the complex frequency response of a material is uniquely determined by its temporal response to a short pulse. Each frequency component contained in the pulse can be treated as an independent signal. The short pulse is thus equivalent to a tunable monochromatic source covering the same range of frequencies.

An example of the implementation of this approach is illustrated in Fig. 4. A material whose dielectric response is desired is placed in contact with the lithium tantalate crystal in which the far-infrared signals are generated and measured. The Čerenkov wave front is then reflected from the interface between the two materials. The probing optical beam measures both the incident waveform and, at a delayed time, the reflected waveform. At first thought, this would appear to provide sufficient information to determine the dielectric response of the material of interest. A difficulty arises, however, because the probing optical pulse measures the in-

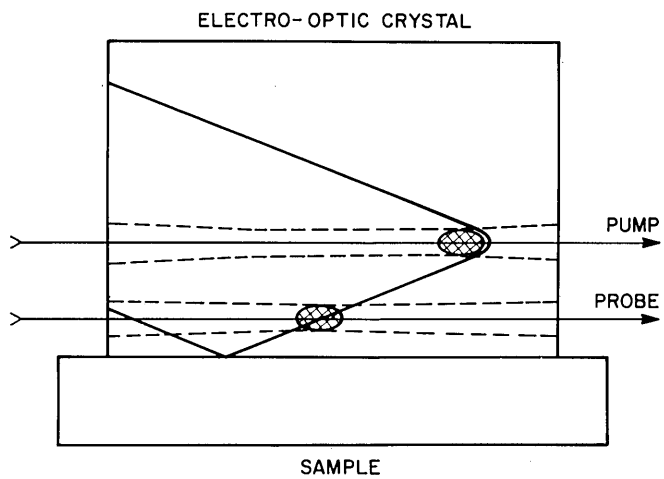

Fig. 4. Schematic of the experimental arrangement used to measure the far-infrared dielectric properties of materials by coherent time-domain spectroscopy. The material to be measured is placed in contact with the electro-optic crystal in which the far-infrared pulses are generated and measured. The Čerenkov wave front is measured by the probing optical pulse before and after being reflected from the interface. The dielectric response of the material is determined by a numerical Fourier transform of the reflected waveform. To calibrate the timing, a reference sample such as a metal film or the open interface is substituted for the sample.

cident and reflected waveforms at a finite distance from the interface. Although this distance can be made relatively small (typically 100 μm), some distortion and attenuation result from propagating through this additional distance in the lithium tantalate. Also, the absolute value of this distance is difficult to determine, which introduces an uncertainty into the timing of the reflected waveform; consequently the phase of its spectrum is not defined. An expedient solution to this problem is to do a second measurement under identical conditions of a reference sample whose dielectric properties are known. For example, this could be a metal film, or, even more simply, the total internal reflection from the air interface (in the latter case a subtlety arises because of an intrinsic dispersion between positive and negative frequencies). This reference waveform accurately defines the timing of the reflection and enables the essential phase information to be determined. Specifically, we determine the reflectivity of the sample at each frequency by the relationship

$$r(\omega) = \frac{\int_{-\infty}^{+\infty} dt E(t) e^{i\omega t}}{\int_{-\infty}^{+\infty} dt E'(t) e^{i\omega t}} r'(\omega), \tag{5}$$

where the unprimed and primed quantities refer to the sample and the reference, respectively. The frequency spectra of the reflected waveforms are determined numerically. The reflectivity of the reference $r'(\omega)$ is calculated from the Fresnel formula for a single interface using its known complex dielectric constant $\epsilon'_2(\omega)$:

$$r'(\omega) = \frac{\cos\theta_i - [\epsilon'_2(\omega)/\epsilon_1 - \sin^2\theta_i]^{1/2}}{\cos\theta_i + [\epsilon'_2(\omega)/\epsilon_1 - \sin^2\theta_i]^{1/2}}, \tag{6}$$

where the subscripts 1 and 2 refer to the electro-optic and reflecting media, respectively, θ_i is the angle of incidence (21 deg in our case), and ϵ_1 is the dielectric constant of the electro-optic material. For the geometry depicted in Fig. 4, the angle of incidence θ_i is the complement of the Čerenkov cone angle θ_c.

Once the reflectivity spectrum of the sample is known, its complex dielectric functions can be determined by inverting the Fresnel reflectivity expression (6) to give the result

$$\frac{\epsilon_2(\omega)}{\epsilon_1} = \sin^2\theta_i + \cos^2\theta_i \left[\frac{1 - r(\omega)}{1 + r(\omega)}\right]^2 \tag{7}$$

The full power of this procedure is apparent in its ability to obtain both the real and the imaginary parts of the dielectric response over a broad range of frequencies from a single waveform (plus a reference). This can be compared with incoherent methods, which measure the magnitude of the reflectivity and must resort to Kramers–Kronig analyses to determine the complex dielectric function. We will return to a discussion of these and related points following a description of some experimental examples.

DIELECTRIC RESPONSE OF A SEMICONDUCTOR PLASMA

We now proceed to illustrate this approach with two examples. The first is the measurement of the dielectric properties of a solid-state plasma in an n-type sample of germanium. The specific sample used for this measurement was an antimony-doped sample of germanium with a nominal resistivity of approximately 0.03 Ω cm. This doping level produces an electron density of approximately 5×10^{16} cm^{-3}, resulting in a plasma frequency within the spectral range spanned by our far-infrared pulses. The incident and reflected waveforms from the sample are shown in Fig. 5 along with the reference waveforms from a gold film. Figure 6 shows an expanded display of these reflected waveforms along with a second reference waveform from the total internal reflection of the open interface. The effect of the reflection from the metal film is seen to produce a waveform that is essentially identical in shape to the incident waveform but is inverted in sign. The open interface produces a reflected waveform that has a phase distortion that is due to the intrinsic singularity at zero frequency of total internal reflection. This phenomenon is a characteristic of monocycle pulses and is discussed in detail in Ref. 10. The n-type germanium produces a severely distorted waveform because of the strong dispersion of the plasma resonance. By using numerical Fourier transforms

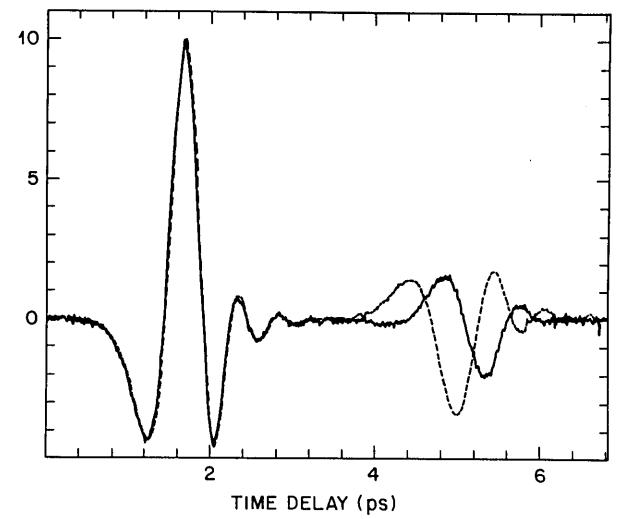

Fig. 5. Reflected waveform from a germanium crystal containing approximately 2×10^{16} cm^{-3} free electrons (solid curve). For comparison, the reflected waveform from a gold film (dashed curve) is also shown.

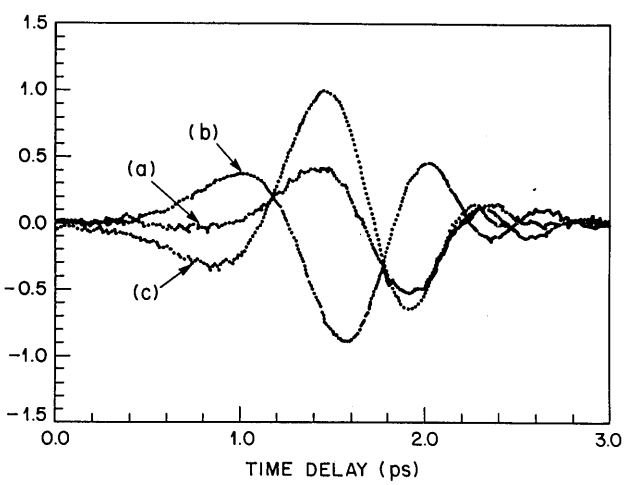

Fig. 6. Expanded view of the reflected waveforms from (a) the n-type germanium sample and (b) the gold film shown in Fig. 5. An additional waveform (c) that is due to the reflection from the open interface is also plotted. The influence of the plasma resonance shows in the strong dispersion, which distorts the reflected waveform.

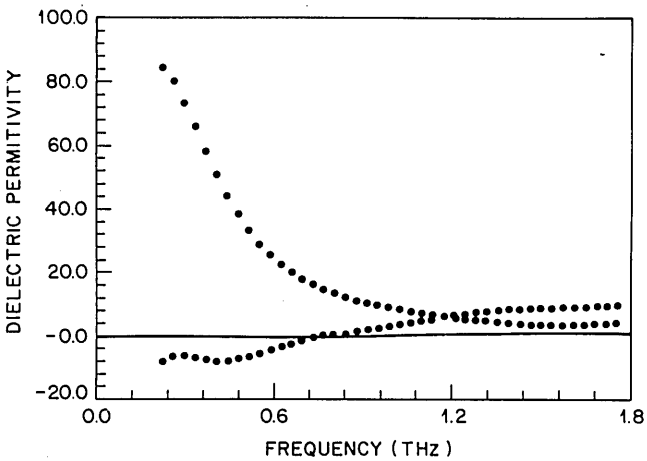

Fig. 7. The real (lower curve) and imaginary (upper curve) parts of the complex dielectric response of the doped germanium sample. These results are obtained by inverting the Fresnel reflection formula using the waveform in Fig. 6 to determine the frequency-dependent reflectivity.

to determine the reflectivity spectra, the complex dielectric function can be determined by the procedure outlined in the previous section. The result is plotted in Fig. 7. The real and imaginary parts follow the expected behavior for a solid-state plasma:

$$\epsilon(\omega) = \epsilon_s - \frac{ne^2}{m^*}\frac{1}{\omega\left(\omega + \frac{i}{\tau}\right)}, \tag{8}$$

where τ is the electron momentum relaxation time, n is the electron density, m^* is the effective mass, ϵ_s is the static dielectric constant, and e is the unit electronic charge. The plasma frequency is defined as the frequency at which the real part of the dielectric function goes to zero and, as shown in Fig. 6, is equal to 0.75 THz in this sample. The large imaginary part of $\epsilon(\omega)$, which diverges at zero frequency, is consistent with a large conductivity. A comparison of the expected behavior of the electron plasma described by Eq. (8) with the experimental data in Fig. 6 enables us to determine the electron density to be 1.6×10^{16} cm^{-3} and the momentum relaxation time to be 225 fsec. From these results the resistivity and the electron mobility are determined to be 0.075 Ω cm and 3300 cm^2/V sec, in good agreement with expected values.

It is interesting to translate the dispersion of the solid-state plasma represented by Eq. (8) into the time domain. Unfortunately, the roots in the Fresnel equation prevent us from deriving an expression for the reflectivity. However, the total current (displacement + polarization) can be written as

$$J(t) = \epsilon_s \frac{\partial E(t)}{\partial t} + \frac{ne^2}{m^*}\int_{-\infty}^{t} dt' E(t')\exp[-(t-t')/\tau]. \tag{9}$$

This result provides some insight into the way in which the pulse shape is distorted. The effect of the plasma is to introduce a convolution with a decaying exponential. The time constant of this exponential factor is determined by the momentum relaxation time τ, and its magnitude is proportional to the electron density. If the relaxation time is very short compared with the pulse duration, the convolution does not appreciably change the shape of the waveform. This is equivalent to the statement that the polarization current in a highly conducting material is "in phase" with the electric field. On the other hand, in a material in which τ is very long, the polarization current is proportional to the integral of the electric field, or is "in phase quadrature" with the electric field.

DIELECTRIC RESPONSE OF A MULTI-QUANTUM-WELL SUPERLATTICE

As a second illustration of the use of coherent time-domain far-infrared spectroscopy, we have measured the dielectric response of electrons confined in a two-dimensional multi-quantum-well superlattice.[10] The GaAs/GaAlAs structure was grown by molecular beam epitaxy and consisted of alternating layers of GaAs and $Ga_{0.79}Al_{0.21}As$ on a chromium-doped semi-insulating GaAs substrate, as shown in Fig. 8. The multi-quantum-well structure was designed so that the dopant electrons from the GaAlAs layers flow into the lower-band-gap GaAs layers, where they are confined in a two-dimensional geometry. The width of the conducting GaAs layers was 242 ± 10 Å. A dopant (silicon) was introduced into the GaAlAs layers with a concentration of approximately 10^{18} cm^{-3}. In this particular superlattice, the dopants were introduced into GaAlAs layers of two different thicknesses, 391 ± 10 and 195 ± 10 Å, as indicated in Fig. 7(a). This resulted in a somewhat more complicated geometry with a fundamental periodicity of 0.147 ± 0.01 μm in which each period contained two conducting GaAs channels, each having an effective areal electron density of approximately 2.93 ± 10^{12} cm^{-2}. There were 10 periods, giving a total thickness of 1.47 ± 0.07 μm.

Figure 9 shows the reflected waveform from the sample. For comparison, the reflection from a semi-insulating chromium-doped sample is also shown. The semi-insulating sample, being essentially nondispersive, produces a reflected waveform that is identical in shape to the incident waveform. The multi-quantum well, however, produces a reflected waveform, which shows dramatically the dispersion that is due to the free carriers.

The dielectric function of a periodic lattice of two-dimensional conducting layers was derived by Fetter[11] and was subsequently discussed in detail for semiconductor multi-quantum-well superlattices by Das Sarma and Quinn.[12] The result is

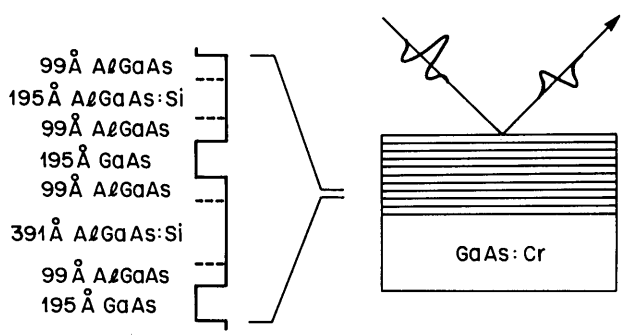

Fig. 8. Composition of the multi-quantum-well superlattice grown by molecular beam epitaxy. The reflected waveforms from this sample are shown in Fig. 9. An effective medium approximation was used to represent the superlattice by a uniform film whose far-infrared properties are determined by the average areal density n_s and momentum relaxation time τ.

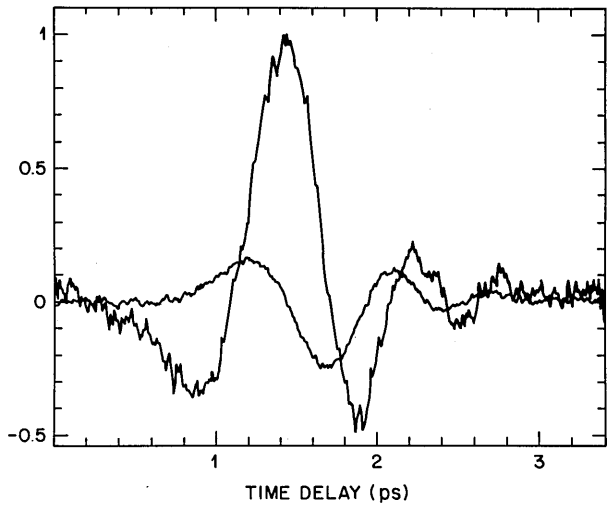

Fig. 9. Reflected waveforms from the multi-quantum-well-superlattice illustrated in Fig. 8 (solid curve) and a bare GaAs:Cr substrate reference (dashed curve), which has been scaled to represent an equivalent incident waveform.

$$\epsilon(\omega, k) = \epsilon_s - \frac{n_s e^2 k_\parallel}{m^*} \frac{1}{\omega\left(\omega + \frac{i}{\tau}\right)} \times \frac{\sinh(k_\parallel a)}{\cosh(k_\parallel a) - \cos(k_\perp a)}, \quad (10)$$

where a is the superlattice period, n_s is the areal electron density, τ is the momentum relaxation time, and $k_\perp$ and $k_\parallel$ are the components of the wave vector perpendicular and parallel to the planes, respectively. In the long-wavelength limit, expression (10) reduces to the dielectric function of a uniform plasma given by expression (8) with an effective electron density equal to n_s/a. This enables us to model the superlattice by an effective medium approximation that represents the multi-quantum wells by a uniform layer with an average electron density n_s/a and a momentum relaxation time of τ. The reflectivity is then determined by the double interface expression

$$r(\omega) = \frac{r_{12} + r_{23} \exp(i2d\sqrt{\epsilon_2} \cos\theta_2)}{1 + r_{12} r_{23} \exp(i2d\sqrt{\epsilon_2} \cos\theta_2)}, \quad (11)$$

where r_{12} and r_{23} are the single interface reflectivities. In our specific case, medium 1 is the lithium tantalate crystal, medium 2 is the superlattice, and medium 3 is the semi-insulating GaAs substrate.

Since expression (11) cannot be inverted, as was possible with the single interface problem discussed in the previous section, we use a curve-fitting procedure to determine the superlattice parameters n_s and τ. To do this we start with the waveform from the bare substrate and determine an incident waveform by scaling its amplitude by the known reflectivity from the $LiTaO_3$–GaAs interface. This reflection is expected to be essentially nondispersive and has the numerical value of 0.415. This incident waveform is then numerically reflected from the superlattice structure by using expression (11) for different values of n_s and τ until the best fit to the experimental reflected waveform is obtained. An extremely good fit was obtained for an areal density of 0.92×10^{11} cm^{-2} and a mobility relaxation time of 190 fsec (assuming an effective mass of 0.067). The areal density is smaller by a factor of approximately 3 than what we expected from the free-carrier concentration. The reason for this discrepancy is not clear. The mobility relaxation time, however, agrees extremely well with Hall measurements on comparable samples (i.e., a mobility of 5050 ± 500 cm^2/V sec).

DISCUSSION

There are some aspects of this approach to far-infrared spectroscopy that deserve further discussion. For example, it is interesting to identify the factors that determine the spectral range and resolution. The most important of these is the spectral content of the generated far-infrared pulses. Although lithium tantalate served well to illustrate the basic properties of this approach described in this paper, it is probable that other electro-optic materials could produce even shorter pulses with greater spectral content. The available optical pulses do not impose a major limitation and are becoming ever shorter as improvements in lasers and compression techniques continue to evolve. The constraint imposed by the finite beam waist is more difficult to overcome.

In the absence of noise, the finite response time of the electro-optic detection process does not directly affect the results for the dielectric function of materials determined by the procedure outlined in this paper. This occurs because the detector response enters as a convolution that modifies the sample and reflected waveforms equally. In the frequency domain this convolution is represented by a spectral filter that multiplies both waveform spectra and hence cancels when we take their ratio to determine the reflectivity by expression (5).

Noise limits the useful spectral range to those frequencies for which the detected signal exceeds the noise level. Since the noise in the sample waveform is not correlated with the noise in the reference waveform, it is indistinguishable from a contribution that is due to the dielectric response. In the experiments that we have described, the signal-to-noise ratio was approximately 100:1. From the pulse spectrum, this would produce an upper-frequency cutoff of approximately 2.5 THz. In practice, however, other factors, such as alignment tolerance, interface flatness, and contrast, often result in a somewhat lower figure.

The equivalent spectral resolution of this approach is determined by the reciprocal of the duration of the temporal window used for the measurement. For example, a 6-psec total scan is equivalent to a spectral resolution of approximately 0.05 THz. Since the scanning range can be readily increased, this resolution can be made even better. A practical constraint owing to multiple reflections of the waveforms in the lithium tantalate crystal would limit the resolution to approximately 0.01 THz (≡0.3 cm^{-1}) for a 1-mm crystal.

Although the signal amplitude used in these experiments (≈10 V/cm) is adequate for most applications to linear spectroscopy, it is clearly possible to increase it greatly by using amplified optical pulses. We estimate that this could produce electric-field amplitudes of 10 to 100 kV/cm without risking optical damage to the electro-optic crystal. This would then enable a wide variety of nonlinear far-infrared measurements to be made, such as nonlinear lattice dynamics, soliton propagation, and electron heating and velocity overshoot in

semiconductors. In addition, the capability to make time-resolved measurements could be extended by using a third optical pulse to produce nonequilibrium excitations in materials that could be probed with both temporal and spectral resolution. These and related aspects of this approach will be explored in subsequent publications.

ACKNOWLEDGMENTS

The authors would like to thank A. C. Gossard and W. Wiegmann for providing the multi-quantum-well superlattice sample and P. R. Smith for technical assistance.

REFERENCES

1. For recent reviews, see *Infrared and Millimeter Waves*, K. J. Button, ed. (Academic, New York, 1983), Vol. 8.
2. D. H. Auston, Appl. Phys. Lett. **43,** 713 (1983).
3. D. A. Kleinman and D. H. Auston, IEEE J. Quantum Electron. **QE-20,** 964 (1983).
4. D. H. Auston, K. P. Cheung, J. A. Valdmanis, and D. A. Kleinman, Phys. Rev. Lett. **53,** 1555 (1984).
5. M. Bass, P. A. Franken, J. F. Ward, and G. Weinreich, Phys. Rev. Lett. **9,** 446 (1962).
6. I. Kaminow, in *Handbook of Lasers*, J. Pressley, ed. (Chemical Rubber Company, Cleveland, Ohio, 1971), Chap. 15.
7. A. S. Barker, Jr., A. A. Ballman, and J. A. Ditzenberger, Phys. Rev. B **2,** 4233 (1970).
8. R. L. Fork, B. I. Greene, and C. V. Shank, Appl. Phys. Lett. **38,** 671 (1981).
9. J. A. Valdmanis, G. A. Mourou, and C. W. Gabel, IEEE J. Quantum Electron. **QE-19,** 664 (1983).
10. R. Dingle, H. L. Stormer, A. C. Gossard, and W. Wiegmann, Appl. Phys. Lett. **33,** 665 (1978); H. L. Stormer, J. Phys. Soc. Jpn. **49A,** 1013 (1980).
11. A. L. Fetter, Ann. Phys. (N.Y.) **88,** 1 (1974).
12. S. Sas Sarma and J. J. Quinn, Phys. Rev. B **25,** 7603 (1982).